Enhancing mechanical and thermal properties of plasticized poly-L-(lactic acid) by incorporating aminated-cellulose nanocrystals

Mohamed Aouay, Albert Magnin, Jean-Luc Putaux, Sami Boufi

Enhancing mechanical and thermal properties of plasticized poly-L-(lactic acid) by incorporating aminated-cellulose nanocrystals

Mohamed Aouay[a*], Albert Magnin[b], Jean-Luc Putaux[c], Sami Boufi[a*]

[a] University of Sfax - LMSE - Faculty of Sciences - BP 802 - 3018 Sfax, Tunisia

[b] Univ. Grenoble Alpes, CNRS, Grenoble INP, LRP, F-38000 Grenoble, France

[c] Univ. Grenoble Alpes, CNRS, CERMAV, F-38000 Grenoble, France

Corresponding authors: e-mail: *Sami Boufi : sami.boufi@fss.rnu.tn*

Published in: **Industrial Crops & Products** 202 (2023), 117011
DOI: 10.1016/j.indcrop.2023.117011

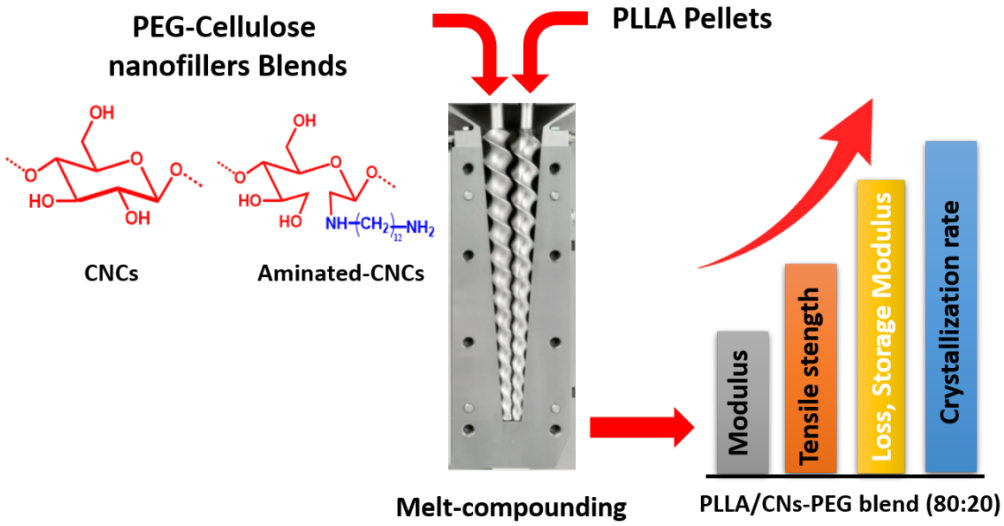

Abstract

Cellulose nanocrystals (CNCs) have attracted much interest as a nucleating and reinforcing agent for poly-L-(lactid acid) (PLLA). However, the processing route to incorporate CNCs into PLLA matrices and the CNCs content have a strong impact on the nucleating and reinforcing efficiency of the cellulose nanofillers (CNs). In the present work, a single melt-processing mode using poly(ethylene glycol) (PEG) as carrier for the CNCs and aminated CNCs (Am-CNCs), prepared via periodate oxidation followed by the addition of diaminododecane, was adopted to elaborate plasticized PLLA composites with different CN contents. The nucleating efficiency was investigated by differential scanning calorimetry using Avrami's approach to determine the half-crystallization time ($t_{1/2}$). The influence of the CNC content on the mechanical properties and melt rheology was also assessed by tensile test and frequency sweep measurements. A significant evolution in tensile strength, modulus and storage modulus in the melt as a function of the CNC content was observed, that was explained in terms of nucleating ability of the CNCs and their dispersion degree within the plasticized PLLA matrix.

1. Introduction

The demand for poly-L-(lactic acid) (PLLA) has been on a steady rise in recent years, especially in the packaging industry where it is increasingly being used as a substitute for petroleum-based polymers. PLLA is a highly versatile and eco-friendly polymer that has gained considerable attention in the last decades due to its unique set of properties. As a thermoplastic aliphatic polyester, it has the potential to biodegrade and compost in certain conditions, making it a sustainable alternative to traditional plastic materials. Additionally, PLLA boasts excellent mechanical properties, such as high modulus and stiffness, which make it an ideal candidate for a wide range of applications, including packaging, medical devices, and textiles. Its transparency and resistance to oil and grease further enhance its appeal, making it a material of choice for manufacturers seeking sustainable and high-performance solutions. (Lunt, 1998; Lim et al., 2008). The exceptional mechanical properties of PLLA make it not only a desirable material but also an easy one to work with. Its processability using conventional thermoplastic processing methods, such as extrusion, injection molding, and thermoforming, enables it to be readily incorporated into existing manufacturing processes (Arao et al., 2015). Despite its enormous potential, PLLA faced several shortcomings when applied to produce flexible products, such as brittleness (strain at break < 3%), poor impact resistance (its impact strength does not exceed 2.5 kJ m^{-2}), poor toughness, and slow crystallization rate (Lim et al., 2008; Soulestin et al., 2011). Another shortcoming of PLLA is its poor crystallization aptitude after melt processing, which is the consequence of its relatively high glass transition temperature (T_g around 60°C). The low degree of crystallization of PLLA results in a poor heat resistance (heat distortion temperature HTD < 55 °C) and low barrier properties against gases (CO_2 and O_2). Therefore, many efforts were made to enhance the crystallization kinetics of PLLA by adding a nucleating agent that reduces the barrier energy for the formation of a stable nuclei with a critical size on which the crystallites of PLLA can grow to form spherulites.

Among the wide variety of available nucleating agents, there is an increasing interest in using nanoscale biobased nanoparticles (NPs) as nucleating agents for PLLA. This interest is motivated by the attributes of biobased NPs, namely, renewable character, non-toxicity, ease to produce, biodegradability, and safety to handle. In particular, the use of NPs with a high-aspect ratio such as chitin (Singh et al., 2020) or cellulose nanocrystals (CNCs) would be beneficial for mechanical properties, thanks to the strong reinforcing effect of CNCs when included in a polymer matrix. This reinforcing effect is the consequence of the high stiffness of CNCs, and their aptitude to generate a percolated network when their content exceeded a critical threshold

between 2 and 3 wt%, depending on their aspect ratio. Several papers have demonstrated the effectiveness of CNCs to act as a nucleating agent for PLLA (Seraji et al., 2022; Clarkson et al., 2020; Yin et al., 2022; Seraji et al., 2022; Wu et al., 2022). However, the processing approach to mix CNCs with PLLA is of paramount importance to take advantage of both the nucleating aptitude of CNCs and their reinforcing effect. Indeed, the beneficial effect of CNCs in PLLA depends on its effective dispersion within the PLLA matrix, and the aggregation of the nanofiller during the processing inevitably results in a loss of these advantages. In many of the reported works on PLLA/CNCs composite, a solvent route has been used, where CNCs suspensions in a polar solvent such as dimethylformamide (DMF) or dimethylacetamide (DMAC) were mixed with PLLA solutions, followed by casting until complete evaporation of the solvent (Niu et al., 2022; Cao et al., 2021). However, this processing route is not viable at an industrial scale and more environmentally friendly approaches should be considered. In this sense, the use of a liquid-feeding strategy or a plasticizer as a carrier opens new ways in melt-processing of PLLA/CNCs composites. In liquid feeding, the CNCs are dispersed in a liquid medium composed of a volatile solvent and a plasticizer and then directly pumped into the extruder during compounding, while in the plasticizer carrier strategy, a water-soluble plasticizer is mixed with a CNCs aqueous suspension, and the dried plasticizer-CNCs blend is compounded with PLLA by melt-extrusion.

In our previous work, the ability of various biobased NPs, having diverse morphologies and surface properties, to act as nucleating agents for PLLA was studied. These NPs included cellulose nanofibrils with and without lignin (LCNFs and CNFs) as well as cellulose, chitin, and starch nanoparticles (CNCs, ChNCs, and SNPs) (Aouay et al., 2022). Films containing 1 wt% of different NPs were prepared using a single melt-processing step where poly(ethylene glycol) (PEG) was used as a carrier for the NPs at a content of 5 wt% with respect to PLLA. According to measurements of surface energy, it was found that the NPs exhibiting the greatest polar component, represented as γ^p, possessed the lowest $t_{1/2}$ and exhibited the most pronounced ability to promote nucleation. (Fortunati et al., 2012; Espino-Pérez et al., 2013; Yu et al., 2017; Aouay et al., 2022).

The present work describes the effect of the inclusion of cellulose nanocrystals (CNCs), namely CNCs and amine-modified CNCs (Am-CNCs), on plasticized PLLA using a one-step melt-processing route, and PEG as both a plasticizer and carrier for CNCs to facilitate the dispersion of CNCs within the PLLA matrix. The Am-CNCs were prepared via periodate oxidation of neat CNCs followed by the addition of dodecanediamine to generate a Schiff base, and finally by reduction of sodium borohydride to reduce the imine group into an amine one.

The CNC and Am-CNC content ranged from 0 to 4 wt%, and the impact of the inclusion of the NPs on the crystallinity, mechanical and melt rheology of PLLA-PEG-NCs composites was studied. To our knowledge, the use of aminated-CNCs as a nucleating agent for PLLA, has so far not been reported in the literature.

2. Materials and Methods

2.1. Materials

Metaperiodate ($NaIO_4$), sodium borohydride ($NaBH_4$), dodecanediamine (DDA) (>98%), and PEG (1000 g mol^{-1}) were purchased from Sigma-Aldrich. CNCs from CelluForce and PLLA pellets (PLE 005-France) from NaturPlast were used to fabricate nanocomposite films.

2.2. Synthesis and of amine-functionalized cellulose nanocrystals

CNCs were functionalized with DDA through a three-step process: (i) 1 g CNCs was oxidized using metaperiodate by dispersing them in 50 mL of deionized water and adding 0.5 g of metaperiodate (corresponding to weight ratio CNCs/$NaIO_4$ of 2/1). The mixture was then heated in a water bath at 40°C under stirring for 48 h in the dark, and the suspension were centrifuged and washed three times with deionized water to recover the oxidized CNCs (ox-CNCs). (ii) 1 g of the ox-CNCs was dispersed in 100 mL of deionized water, and the pH was adjusted to 4.5 by addition of a 10^{-3} M HCl solution. 1 g of DDA was added and kept under stirring at 80 °C for 24 h to form the imine. (iii) 0.5 g of $NaBH_4$ was progressively added to reduce the imine into amine and kept under stirring at room temperature for 2 h. After centrifugation, the suspension was dialyzed until the conductivity of the dialysis medium remained constant, to remove the unreacted amine and the residual salts. The resulting product will be referred to as Am-CNCs in the following.

2.3. Transmission electron microscopy (TEM)

Droplets of dilute CNC and Am-CNC aqueous suspensions were deposited onto glow discharged carbon-coated copper grids and stained with 2 wt% uranyl acetate before drying. The specimens were observed with a JEOL JEM-2100 Plus microscope operating at 200 kV and images were recorded with a Gatan Rio 16 camera.

2.4. ^{13}C CP/MAS solid-state NMR spectroscopy

The CNC and Am-CNC suspensions were dried into thin films, ground into a powder, packed into zirconia rotors, and analyzed with a Bruker Avance III 400 MHz spectrometer (^{13}C frequency of 100.6 MHz) using cross-polarization (CP) and magic-angle spinning (MAS), at a 12 kHz spinning speed, a sweep width of 29761 Hz, and a recycle delay at 2 s. Each spectrum was averaged over 6000 scans. The ^{13}C chemical shifts were calibrated with glycine (carboxyl group at 176.03 ppm).

2.5. Nanocomposite processing

The compounding process involved blending PLLA with dry CNCs/PEG and Am-CNCs/PEG solid particles in a twin-screw DSM-Xplore15cc Micro-compounder at 190 °C and 100 rpm for 5 min. Prior to compounding, suspensions of CNCs and Am-CNCs with PEG were prepared to produce the CNCs/Am-CNCs-PEG blends. In order to achieve a homogenous dispersion, the CNC and Am-CNC suspensions were subjected to sonication at 70% amplitude (Sonics Vibracel-Model CV-33) for 1 min before being combined with PEG. Afterward, the resulting mixture was dried for 24 h at 45 °C and then manually milled into small particles to facilitate further processing. The nanocomposite film was processed using a flat sheet die with a 3 0.15 mm^2 rectangular cross-section after feeding PLLA and CNCs/Am-CNCs-PEG pellets together into the extruder. The PLLA to PEG weight ratio was maintained at 80:20 throughout the experiment, while the concentration of CNCs and Am-CNCs in the PLLA/PEG blend was altered from 0 to 4 wt% in proportion to the weight of the blend.

2.6. Differential scanning calorimetry (DSC)

Thermograms were obtained using a Perkin-Elmer differential scanning calorimeter (DSC) under a dry N_2 atmosphere. Each sample, weighing approximately 7 mg, was hermetically sealed in an aluminum pan. The samples were subjected to a heating-cooling-reheating cycle, starting from 25 °C and up to 200 °C, followed by cooling back to 25 °C and reheating at a constant rate of 10 °C min^{-1}.

$$X_c(\%) = \frac{100.(\Delta H_m - \Delta H_{cc})}{\Delta H_m^0 . m_{PLLA}} \qquad \textbf{(1)}$$

The degree of crystallinity X_c was calculated using **Eq. 1**, which takes into account the melting enthalpies (ΔH_m) and the cold crystallization (ΔH_{cc}) of the sample, as well as the melting enthalpy of 100% crystalline PLLA (ΔH_m^0 = 93.1 $J.g^{-1}$) and the weight fraction of PLLA (m_{PLLA}) in the nanocomposite.

Details about isothermal crystallization and Avrami analysis via Origin plugin developed by Lorenzo et al. (2007) can be found in the supplementary material.

2.7. Scanning electron microscopy (SEM) of the nanocomposites

The films were fractured in liquid nitrogen, sputter-coated with Au/Pd and the morphology of the cross-section was observed by SEM. Secondary electron images were recorded with a Thermo Scientific Quanta 250 microscope operating at 2.5 kV and equipped with a field-emission gun.

2.8. Tensile properties

Tensile tests were carried out at 25 °C and 35% relative humidity with an Instron testing machine equipped with a load cell with a 100 N maximum capacity. Each sample had five specimens (10 mm × 50 mm) with a thickness of around 200 µm, and a cross-head speed of 5 mm min^{-1} was employed.

2.9. Melt rheology

The rheological properties of PLLA/PEG/CNCs and PLLA/PEG/Am-CNCs nanocomposites were investigated at 190°C using an ARES-G2 TA Rheometer with a plate-plate geometry (25 mm in diameter and 0.5 mm gap). The loss and storage modulus were measured as a function of frequency in the 0.1–10 Hz range.

3. Results and Discussion

3.1. Colloidal properties and morphology of CNCs and Am-CNCs

The Am-CNCs was prepared by periodate oxidation of CNCs followed by treatment with DDA that condensates with the aldehyde groups, generating a Schiff base that is reduced by adding $NaBH_4$ to reduce the imine groups to amine ones (**Scheme 1**). The objective of the reduction was to avoid any risk of hydrolysis of the imine groups through the reverse reaction.

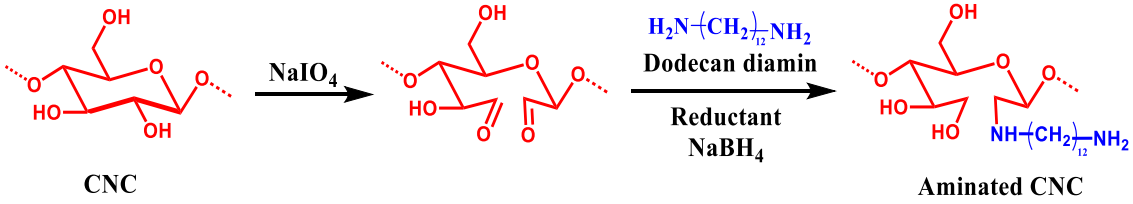

Scheme 1: Synthesis route for the preparation of the amino-modified CNCs (Am-CNCs) through periodate oxidation of CNCs followed by reductive amination with DDA.

The confirmation of the grafting of the amino group was provided by ^{13}C CP/MAS NMR analysis of the Am-CNCs. In comparison with the spectrum of the neat CNCs, an additional large peak between 20-30 ppm, typical of the aliphatic group of the grafted DDA, was observed. The resonances of the carbon atoms of the glucose ring (C_1, C_2-C_3-C_5, C_4, and C_6) were identified by the signals at δ = 104.67, 71.30-74.70, 88.49 and 64 ppm, respectively **(Fig. 1A)**. Each of the C6 and C4 signal was split in two peaks at 64/62 ppm and 88/83 ppm, respectively, assigned to the crystalline and disorganized phase of cellulose in the CNCs. No evolution on the position and intensity of the carbon of the glucose ring of the cellulose were observed after the amination reaction, which indicates that the oxidation and grafting of the amine was restricted to the CNC

surface. A chemical evaluation of the content of amino groups by conductometric titration using NaOH solution, gave a concentration around 380 µmol g^{-1} of CNCs (**Fig. S1**). This content is quite low, meaning that the grafting of DDA only occurred on a limited number of positions on the CNC surface. However, even though the grafting degree was low, a marked reduction in the hydrophilic character of the Am-CNCs was observed, as attested by the increase in the water contact angle, from about 40° for the neat CNCs to 63° for Am-CNCs (**Fig. 1B**).

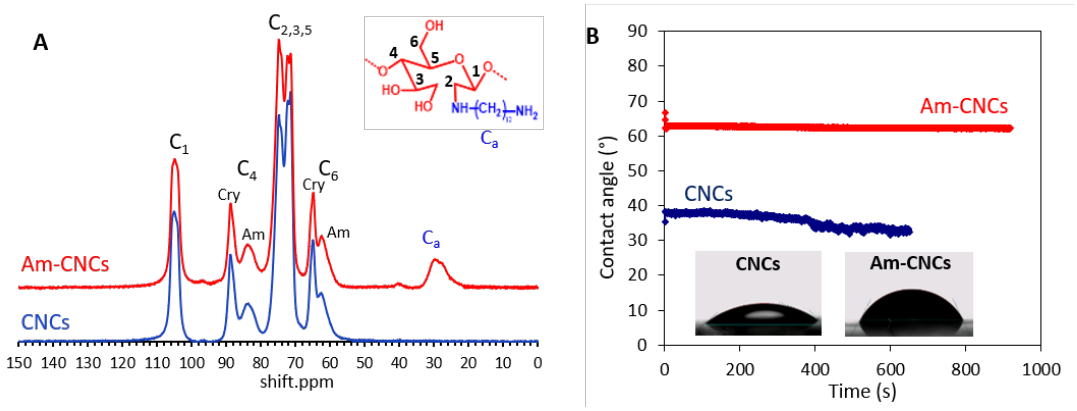

Figure 1. (A) ^{13}C CP/MAS NMR spectra of CNCs and Am-CNCs; (B) contact angle of water on CNC and Am-CNC films (Cry and Am refer to the crystalline and amorphous fractions).

TEM images of CNCs showed polydisperse rodlike objects constituted of a few laterally associated elementary crystallites which were not separated throughout the preparation process (**Fig. 2A**). The average dimensions of CNCs were 13 ± 7 nm in width and 188 ± 86 nm in length, in agreement with those reported for CNCs produced by CelluForce (Reid et al., 2017). The amination of CNCs did not change the morphology of the particles but a tendency to flocculate to some extent was detected from the TEM images (**Fig. 2B**). A possible reason would be the presence of the grafted dodecane hydrocarbon chains that decrease the hydrophilic character of the Am-CNCs, as confirmed by contact angle measurement (**Fig. 1B**).

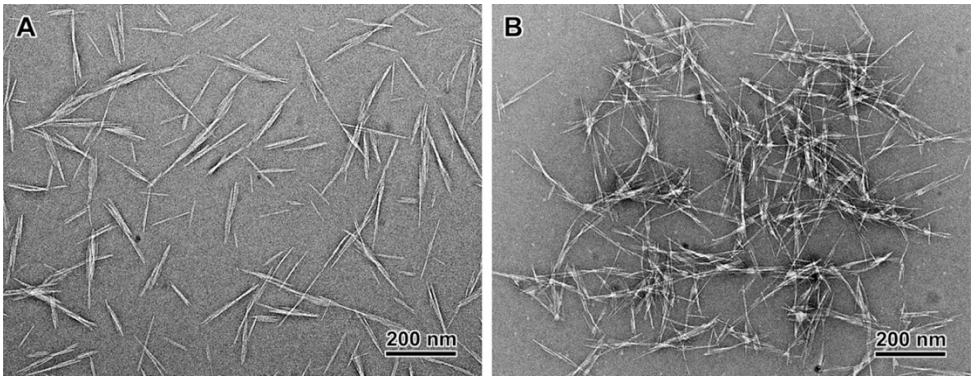

Figure 2. TEM images of negatively stained preparations of CNCs (A), and Am-CNCs (B).

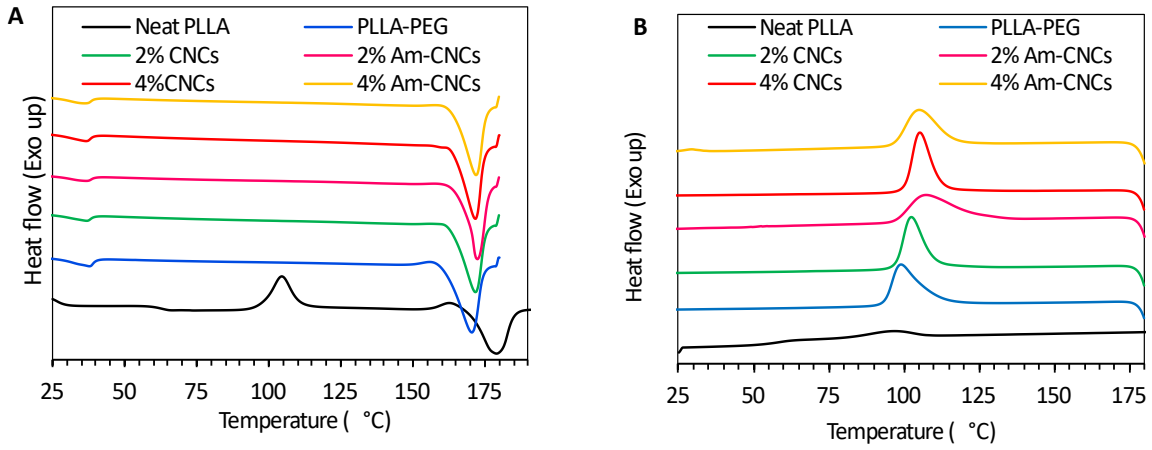

Figure 3. (A) First heating DSC scans, and (B) cooling thermograms of neat PLLA and PLLA/PEG films, as well as PLLA/PEG/CNCs and Am-CNCs nanocomposites.

Table 1. Thermal properties from DSC experiments: glass transition temperature (T_g), temperature of crystallization peak (T_c), temperature of cold crystallization peak (T_{cc}), temperature of melting peak (T_m), cold crystallization enthalpy (ΔH_{cc}), melting enthalpy (ΔH_m) and degree of crystallinity (X_c).

Sample	T_g (°C)	T_{cc} (°C)[a]	T_c (°C)[b]	T_m (°C)[c]	ΔH_{cc} (J g^{-1})	ΔH_m (J g^{-1})	X_c (%)
Neat PLLA	62.2	104.8	-	179	35.0	45.0	10.8
PLLA-PEG	35.2	-	97.1	170	-	33.2	44.5
2% CNCs	35.8	-	101.5	173	-	37.3	50.0
2% Am-CNCs	36.1	-	107.3	173	-	39.8	53.5
4% CNCs	36.0	-	105.1	172.5	-	38.0	51.1
4% Am-CNCs	36.2	-	105.2	172	-	38.4	51.5

[a] T_{cc} temperature of cold crystallization
[b] T_c temperature of crystallization upon cooling
[c] T_m temperature of crystallization upon cooling

3.2. DSC analysis of the PLLA-PEG-CNCs/Am-CNCs nanocomposites

Figure 3A,B shows DSC thermograms of neat PLLA, PLLA/PEG and PLLA/PEG/CNCs nanocomposites at 2 and 4 wt% CNC and Am-CNC contents, respectively. All thermal properties data are collected in **Table 1**. During the first scan, only neat PLLA presents a cold crystallization peak at 105°C, while the other compositions only show a melting peak between 173-179 °C (**Fig. 3A**). This indicates that neat PLLA was not well crystallized after the extrusion, while plasticized PLLA and composite films were able to crystallized after processing. During cooling, all films, with the exception of neat PLLA, exhibited a crystallization peak in the range of 97-106 °C (**Fig. 3B**). The crystallinity degree of neat PLLA was around 10 %, proving its poor

aptitude to crystallization. With the inclusion of 20 wt% PEG-plasticizer, X_c considerably increased to 44%, indicating the potential effect of PEG to promote the crystallization of PLLA, most likely by facilitating the chain mobility. This result is consistent with our previous and other works (Aouay et al., 2022; Clarkson et al., 2020). The addition of CNCs increased X_c to 50-51% at a content of 2 and 4 wt%, confirming the nucleating ability of CNCs. A shift to a higher T_c (+4 to 9 °C, respectively), with respect to the matrix, was also observed, which suggests that by acting as a nucleating agent, CNCs had a considerably positive impact on the kinetics of PLLA crystallization upon cooling.

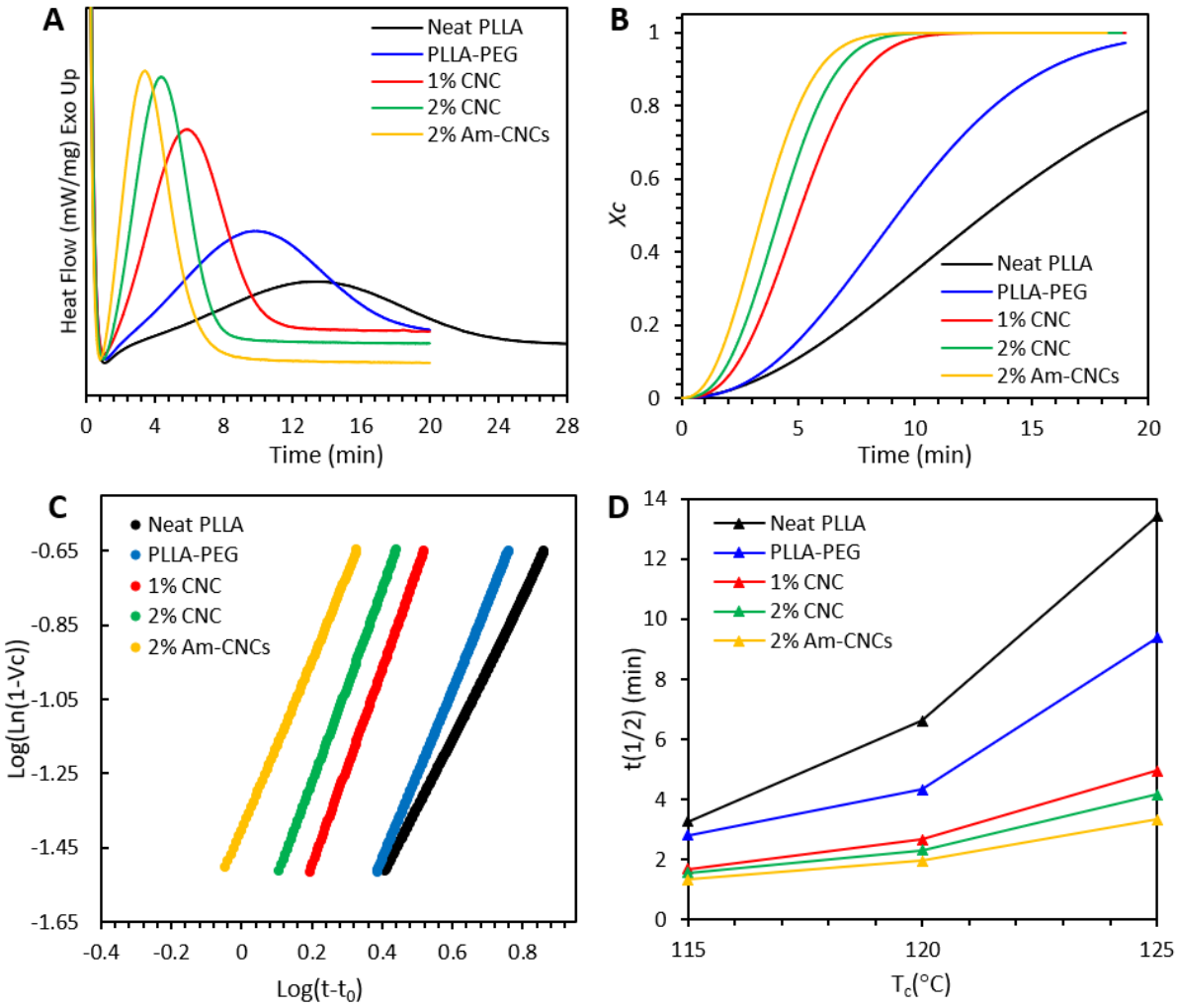

Figure 4. Avrami analysis from isothermal data at 125°C: (A) DSC curves for the isothermal crystallization. (B) the relative crystallinity versus time, (C) Avrami double-log form plot. and (D) half-time, $t_{1/2}$, with T_c for neat PLLA, PLLA/PEG and PLLA/PEG with 1 and 2 wt% CNCs and 2 wt% Am-CNCs.

Table 2. Summary of isothermal crystallization data for neat PLLA, PLLA/PEG, PLLA/PEG/CNCs, and PLLA/PEG/Am-CNCs nanocomposites obtained from Avrami's model at various temperatures.

Sample	T_c (°C)	k $(min^{-1})^n$	n	$t_{½}$ (min)
Neat PLLA	115	3.03×10^{-2}	2.64	3.27
	120	8.10×10^{-3}	2.36	6.61
	125	5.05×10^{-3}	1.90	13.40
PLLA-PEG	115	5.99×10^{-2}	2.40	2.81
	120	2.40×10^{-2}	2.31	4.33
	125	3.94×10^{-3}	2.31	9.38
1% CNCs	115	1.65×10^{-1}	2.72	1.68
	120	4.66×10^{-2}	2.72	2.66
	125	9.80×10^{-3}	2.73	4.96
2% CNCs	115	2.20×10^{-1}	2.77	1.51
	120	7.11×10^{-2}	2.68	2.30
	125	1.59×10^{-2}	2.59	4.16
2% Am-CNCs	115	3.29×10^{-1}	2.38	1.33
	120	1.34×10^{-1}	2.32	1.95
	125	3.91×10^{-2}	2.29	3.33

3.3. Isothermal crystallization kinetics: Nucleating efficiency of CNCs and Am-CNCs

Isothermal crystallization kinetics of neat PLLA, PLLA/PEG, PLLA/PEG/CNCs, and PLLA/PEG/Am-CNCs nanocomposites were investigated using Avrami's theory in order to fully understand the effect of the incorporation of CNCs and Am-CNCs on the crystallization rate of PLLA. The isothermal thermograms presented in **Fig. 4A** highlight the effectiveness of CNCs and Am-CNCs on narrowing the time interval of PLLA crystallization. From the heat of crystallization *vs.* time, and using Avrami's analysis, the relative crystallinity conversion (χ_c) was calculated and the evolution of χ_c *vs.* time showed a typical sigmoid. shape at the different temperature investigated, as depicted in **Fig. 4B** at 125°C and in **Fig. S1** at 120 and 115°C. The time required to complete 50% of the crystallization process is referred to as the half-crystallization time ($t_{1/2}$), and is estimated using **Eq. S5**.

To fully describe the crystallization rate, the contribution of both nucleation and growth rates should be considered. The resulting combined rate is expressed as k, and it provides a measure of the kinetics of crystallization. **Table 2** collects data obtained from Avrami's model for different compositions at various crystallization temperatures.

From the data in **Table 2**, the progression in the evolution of crystallization time and rate is clear. The trend can be observed as follows: PLLA exhibits the longest crystallization time and the slowest crystallization rate, followed by PLLA/PEG, PLLA/PEG-1%CNCs, PLLA/PEG-2%CNCs, and finally PLLA/PEG-2%Am-CNCs, which shows the shortest crystallization time and the fastest crystallization rate.

The isothermal crystallization kinetics of the various compositions were analyzed, and the half-crystallization time ($t_{1/2}$) was determined. The results showed that the addition of PEG and CNCs decreased the $t_{1/2}$ of PLLA, indicating an increase in the crystallization rate. At 125°C, the $t_{1/2}$ for neat PLLA was 13.4 min, while for PLLA/PEG, PLLA/PEG-1%CNCs, PLLA/PEG-2%CNCs, and PLLA/PEG-2%Am-CNCs, it decreased to 9.38, 4.96, 4.16, and 3.33 min, respectively. This demonstrates that the incorporation of Am-CNCs resulted in the fastest crystallization rate among all the compositions studied.

The decrease of the crystallization time with addition of PEG is explained by the plasticizing effect of PEG, that increases the mobility of macromolecular chains, facilitating the packing of PLLA chains within the lamellar crystallites. The inclusion of 1 wt% CNCs markedly decreased the crystallization time, confirming the strong nucleating effectiveness of CNCs for PLLA. The incorporation of 1 wt% CNCs into PLLA/PEG resulted in a significant decrease in $t_{1/2}$ at 125°C, while further increasing the CNCs content to 2 wt% did not result in a substantial change. This indicates that a low CNC content is sufficient to promote the nucleation of PLLA. Interestingly, the addition of 2 wt% Am-CNCs resulted in a much greater reduction in $t_{1/2}$, indicating that a low degree surface modification of CNCs with DDA enhanced the nucleation efficiency of the NPs. The efficiency of CNCs as a nucleating agent for PLLA has also been demonstrated in other works (Shuai et al., 2020, Kulinski and Piorkowska, 2005).

3.4. Mechanical properties

The mechanical properties of the films were investigated by tensile tests at 25°C. The typical stress-strain curves of the PLLA/PEG, PLLA/PEG/CNCs and PLLA/PEG/Am-CNCs at different CNs content are shown in **Figure 5A,B** from which the relevant mechanical characteristics were extracted and presented in **Figure 5C,D**. The inclusion of PEG in PLLA resulted in a significant drop in both the tensile modulus E and ultimate strength (US), which decreased from 3.7 GPa/55 MPa for neat PLLA, to 0.41 GPa/11.2 MPa for PLLA-PEG. This reduction in stiffness was accompanied by an increase in ductility, with an elongation at break ε around 3% (data not shown) to more than 100% for plasticized PLLA. This evolution was expected due to the effective plasticizing action of PEG and its ability to interact with PLLA

chains, thus reducing the polymer-polymer contact and increasing the chain mobility. The incorporation of CNCs and Am-CNCs resulted in a marked evolution in the mechanical properties, with an effect that strongly depended on the CN content, as shown in **Fig.5C,D**. At 1 and 2 wt% CN content, the stiffness and strength of the composite was markedly enhanced with an increment in E/US with respect of the unfilled PLLA/PEG matrix of about 154/106; 420/190% for CNCs and 193/130%, 440/220% for Am-CNCs, at 1 and 2 wt% nanofiller, respectively. However, at a CN content of 4 wt%, a marked decrease in E and US was observed for both CNCs and Am-CNCs in comparison with 2 wt% content. Interestingly, the ductility of the nanocomposite was preserved at 1 and 2 wt% CN content for CNCs as well as Am-CNCs, but notably dropped at 4 wt% CN content. To explain the evolution of the mechanical properties of the PLLA-PEG-CNCs with the CN content, we assumed that the incorporation of CNCs promoted a reinforcing effect, due to their high stiffness (E exceeding 100 GPa), and their aptitude to set-up a percolated network. However, referring to the percolation concept for CNCs, the set-up of percolated network took place above a critical threshold which could be estimated by **Eq. 7** (Samir et al., 2004):

$$\phi_p = \frac{0.7}{L/d} \qquad (7)$$

Assuming a mean value for L, and d about 190 and 13 nm, respectively, based on TEM observation (**Fig. 2**), the expected value of ϕ_p should be around 0.04, which corresponds to a 6 wt% content. This value exceeds by far the content at which the highest enhancement in E and US was observed (i.e. 2 wt% CNC content), meaning that the hypothesis of the set-up of a percolated network should be excluded to explain the reinforcing effect induced by the addition of 1 and 2 wt% CNCs and Am-CNCs. Another reason justifying the improvement in mechanical properties in PLLA/PEG is the nucleating effect induced by the presence of CNs. Indeed, as demonstrated in section 2, and referring to our previous work (Aouay et al., 2022), CNCs have a significant nucleating effect when included in a PLLA matrix. Thanks to their nanosize and rodlike morphology, a content of 1 or 2 wt% would provide a huge number of NPs acting as a nucleating site for PLLA, which is enough to accelerate the growth kinetics of polymer crystallites and spherulites. This hypothesis was confirmed by the huge increase in the crystallinity degree of the matrix containing CNs, reaching about 50% and 53% in the presence of 2 wt% CNCs and Am-CNCs, respectively. However, at 4 wt% CN content, the crystalline degree of the matrix remained similar to that reached at 2 wt% CN content. This result suggests that the enhancement in the crystallinity of PLLA is not the only reason accounting for the marked enhancement in the mechanical properties of the plasticized PLLA containing 1 and 2

wt% CNCs or Am-CNCs. The specific interaction between the nanofiller and the PLLA matrix also affected the reinforcing effect of the nanofiller. This effect may also be the consequence of the better dispersion of the nanofiller induced by the surface modification.

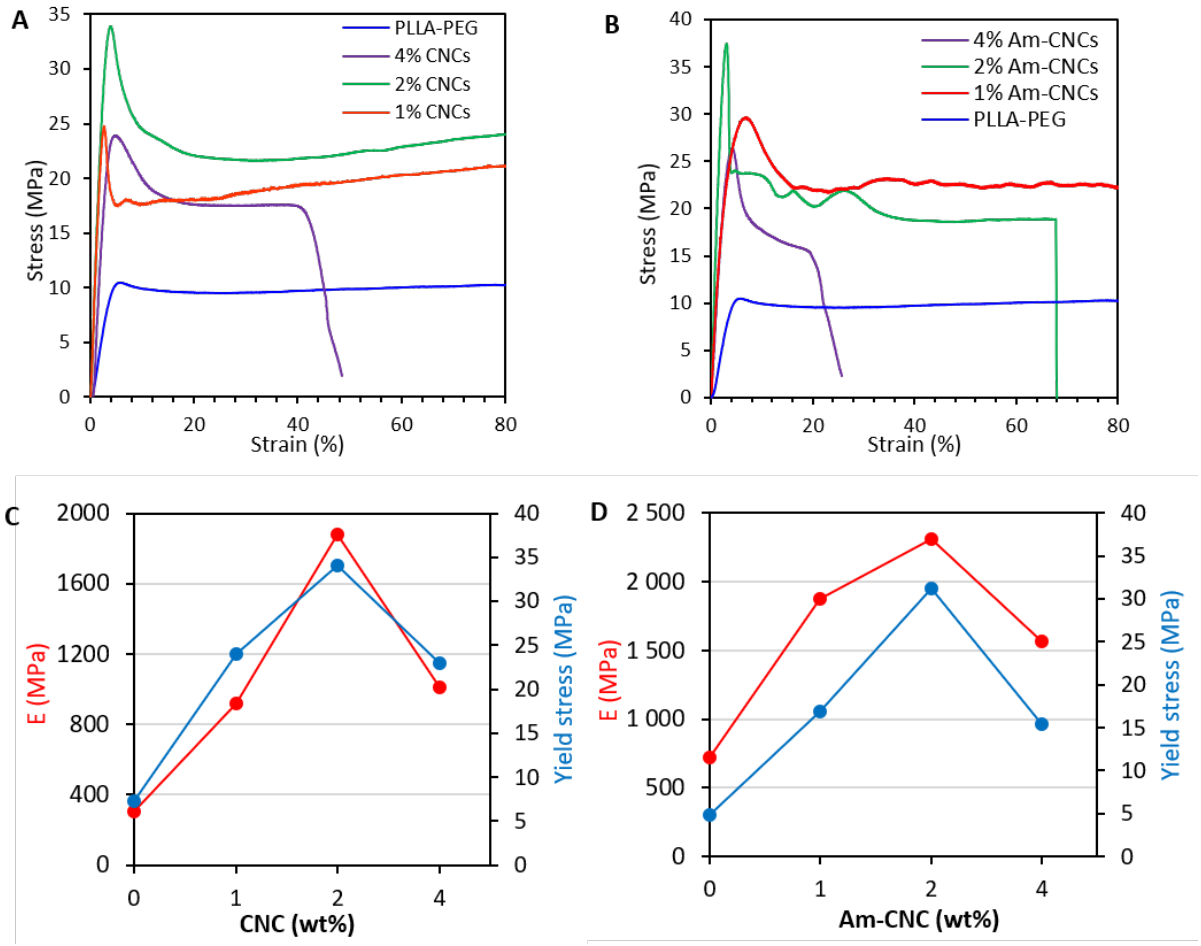

Figure 5. (A) Stress-strain plots of PLLA/PEG, PLLA/PEG/CNCs, (B) PLLA/PEG/Am-CNCs. Young modulus and yield strength *vs.* nanofiller content for (C) PLLA/PEG/CNCs, and (D) PLLA/PEG/Am-CNCs nanocomposites.

In the present work, the decrease in mechanical properties of PLLA/PEG/CN composites over a 2 wt% CN content was explained by the higher degree of CN aggregation. This hypothesis was confirmed by SEM images of the cross-sections of cryofractured films. Although the fraction of well-dispersed particles cannot clearly be detected when embedded in the polymer matrix, a number of CNC or Am-CNC aggregates was seen in all films (**Fig. 6A,B**). At 2 wt% CN content, polydisperse aggregates appeared to be evenly distributed in the matrix, the size of the measurable ones typically ranging from 0.5 to 7 µm (**Fig. S3**). Smaller aggregates likely existed but their size was more difficult to evaluate from the images. At 4 wt% CN content, the aggregates were even more polydisperse, some of them reaching 20 µm in size (**Fig. 6C,D**).

However, since the aggregation was assessed from fracture surfaces, it was difficult to quantify with precision the fraction of aggregated particles with respect to the whole amount of incorporated CNs. The presence of large aggregates will inevitably induce the premature breaking of the composites by acting as a stress concentrator, which explains the steep decrease in the ultimate strength of the film at 4% CN content.

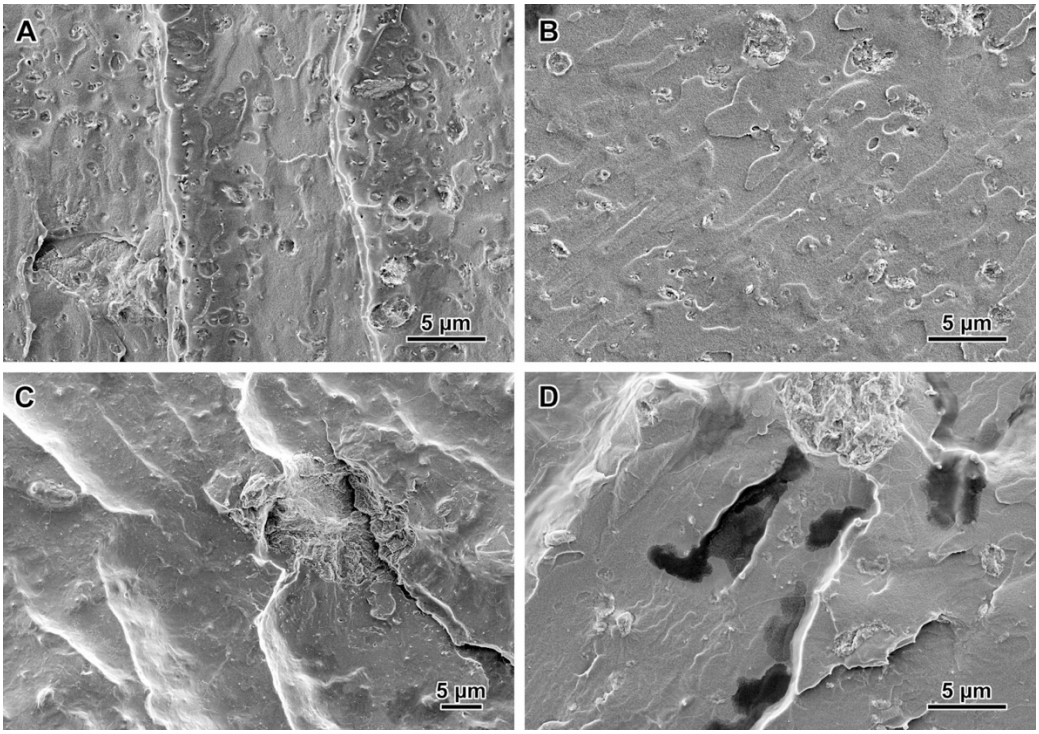

Figure 6: SEM images of the cross-sections of cryofractured PLLA/PEG composite films: (A) 2 wt% CNCs, (B) 2 wt% Am-CNCs, (C) 4 wt% CNCs, and (D) 4 wt% Am-CNCs.

3.5 Rheological properties and CNCs dispersion

To further understand how the inclusion of a cellulose nanofiller in a PLLA/PEG matrix influences the processing characteristics and the viscoelastic properties of PLLA-PEG under melt conditions, an amplitude sweep measurement of the storage (G′) and loss modulus (G″) at 190°C was conducted in the linear regime (**Figure 7**). The rheological behavior of the PLLA/PEG matrix is typical of molten polymer dominated by the viscous character, as evidenced by the higher magnitude of G″ compared with G′ (G″ is about ten-times G′). In the presence of CNCs and Am-CNCs, the melt rheology of the PLLA/PEG blend changes considerably depending on their content. At a nanofiller content of 1 and 2 wt%, both G′ and G″ increased steadily with respect to the neat PLLA/PEG matrix, meaning that the presence of the nanofiller, even at low amount induces a huge increase in the viscoelastic properties of the melt

matrix. This effect is even more pronounced in the presence of Am-CNCs than CNCs. However, at a 4 wt% nanofiller content, G′ and G″ were shifted to lower values in comparison with 2 wt% CN content. The rodlike morphology of the CNs, and their nanosize might justify the huge increase in G′ and G″ up to 2 wt% CN content. The occurrence of aggregation over this content would reduce the number of particles and inevitably lead to a decrease in magnitude of G′ and G″, which might justify the data observed at 4% CN content. The higher magnitude of G′ and G″ observed for Am-CNCs in comparison with CNCs means that the former induces more rigidification of the PLLA/PEG matrix under melt at 2 wt% CN content. Two hypotheses are likely to explain this difference; (i) better dispersion of Am-CNCs in the PLLA-PEG matrix than CNCs, and (ii) higher interaction between PLLA and the nanofiller, presumably through the pendant dodecane amine group of Am-CNCs.

For all compositions, the viscoelastic properties were still dominated by a liquid-like character with G″ about one order of magnitude higher than G′. For the neat PLLA-PEG matrix, a power-law dependence of G′ and G″ with the frequencies, with a regression coefficient R^2 exceeding 0.99, was noted for all the compositions, with $G' \sim f^{2.1}$ and $G'' \sim f^{0.99}$, which is close to the theoretical exponent values of 2 for G′ and 1 for G″. In presence of CNCs or Am-CNCs, the power law index of G′ *vs. f* decreased from 2.1 for PLLA-PEG to 1.76, 1.55 and 1.65 at a nanofiller content of 1, 2, and 4%, respectively, which indicates a rigidification of the polymer under melt state with the inclusion of CNs.

3.6. Optical properties

The optical transparency of PLLA/PEG/CNs nanocomposites was assessed by transmittance measurement in the visible domain of thin film, normalized to a 200 μm thickness using the Beer–Lambert law to eliminate any fluctuation in the transmittance resulting from evolution in film thickness (**Fig. 8**). The unfilled PLLA/PEG exhibits a high degree of transparency as attested by the transmittance exceeding 90% over the whole visible domain from 400 to 800 nm. With the increase in NC content, the transmittance progressively decreased, from 96% at $\lambda = 600$ nm for a pure PLLA/PEG film to 90, 85 and 80% at 1, 2 and 4 wt% CN content, respectively, and 88, 82, and 76%, in the presence of Am-CNCs at a respective content of 1, 2, and 4 wt%. The decrease in transparency with increasing CN content is likely due to the contribution of two effects: on the one hand, the higher crystallinity of the matrix induced by the nucleating effect of the CNs, and, on the other hand, to the aggregation of CNs. Both of these effects promote light scattering, and consequently reduce the fraction of transmitted light.

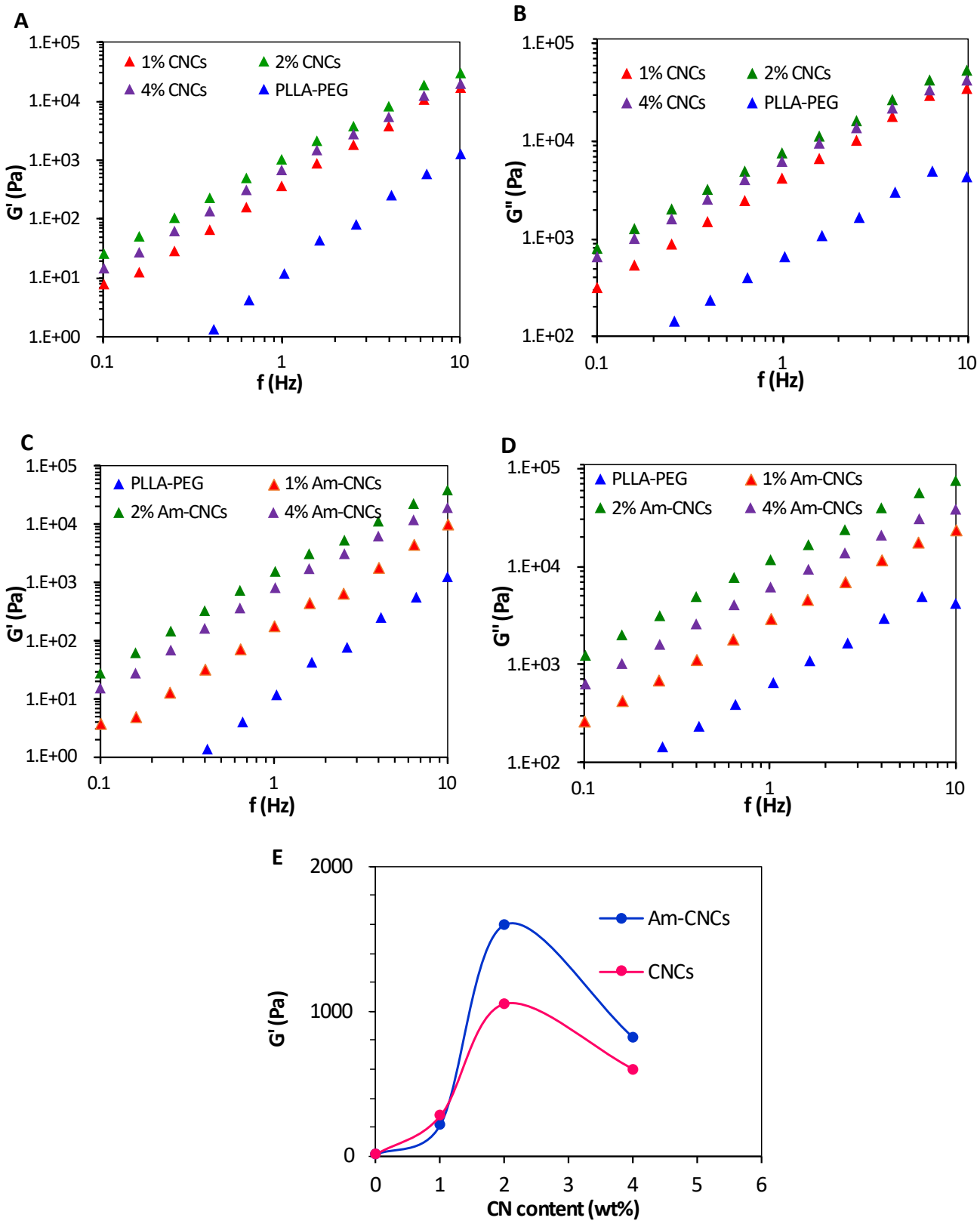

Figure 7. (A,C) Storage modulus (G′), (B,D) loss modulus (G″) *vs.* frequencies (f), at 190 °C of PLLA/PEG and PLLA/PEG/CNs (CNs=CNCs and Am-CNCs), and (E) G' at 1 Hz *vs.* CN content.

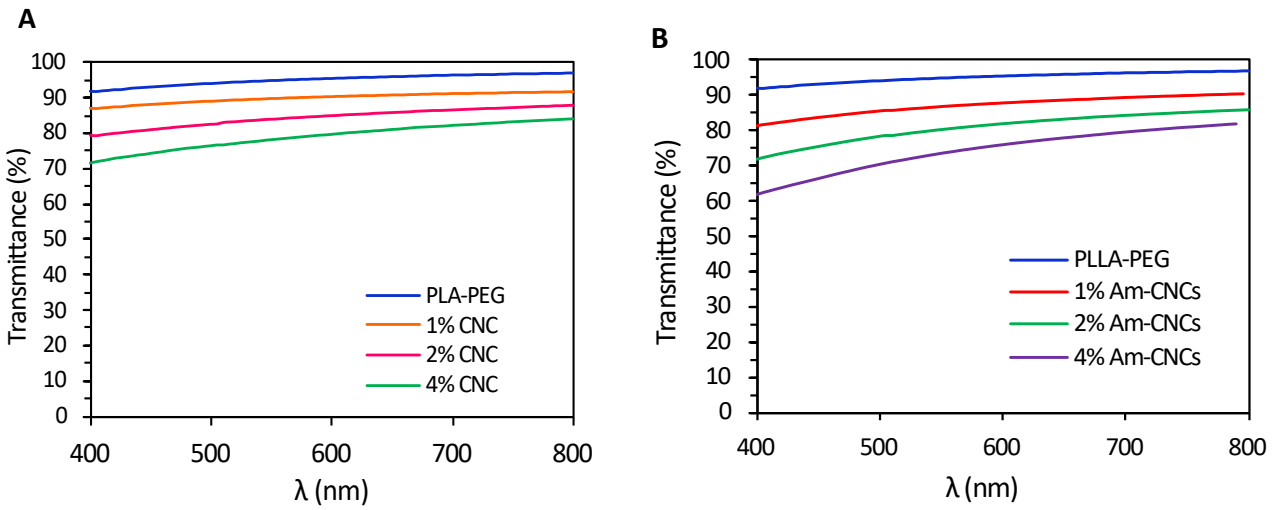

Figure 8. Transmittance in the visible domain of PLLA-PEG films with different content in CNs: (A) CNCs, and (B) Am-CNCs.

4. Conclusions

The present work demonstrates the effective role of PEG as carrier for CNs in a PLLA matrix. Using neat CNCs and aminated CNCs (Am-CNCs) as additive into PEG-plasticized PLLA at a content of 1, 2 and 4 wt%, and adopting a one-step melt processing to prepare the nanocomposite, a substantial enhancement in both tensile strength and tensile modulus increased were noted with, an optimum effect at 2 wt% CNs. This result was observed for both CNCs and Am-CNCs, and at 4 wt%, a decrease in mechanical properties was noted, in comparison with 2 wt% CN loading. A similar tendency was observed for the melt rheological properties, where an increment in G′ and G″ was noted in comparison with the PLLA-PEG matrix, with a maximum at 2 wt% CNs, and a decrease of G′ and G″at 4 wt%. These results were explained by the evolution of the degree of dispersion of the CNs depending on their content. At 1 and 2 wt%, the aggregation was limited, and both CNCs and Am-CNCs effectively accelerated the crystallization kinetics of the PLLA matrix, which explains the huge enhancement in the modulus and strength of the nanocomposites. The decrease in mechanical properties at 4 wt% CN content was explained by the aggregation of CNCs and Am-CNCs when their content exceeded 2 wt% value. This hypothesis was supported by SEM observation of the fractured surface.

Acknowledgements

The authors acknowledge LabEx Tec 21 (Investissements d'Avenir #ANR-11-LABX-0030), as well as the PHC Utique 19G1123 and Glyco@Alps programs (Investissements d'Avenir #ANR-15-IDEX-02) for financial support. We thank the NanoBio-ICMG Platform (UAR 2607, Grenoble) for granting access to the Electron Microscopy and NMR facilities. We thank Christine Lancelon-Pin (CERMAV) for the SEM observations, and Patricia Chaud (CERMAV) for the solid-state NMR analysis. The Partenariat Hubert Curien (CMCU project: 23G1118) is gratefully acknowledged for its financial support. CERMAV and LRP are part of Institut Carnot PolyNat (Investissements d'Avenir #ANR-11-CARN-030-01).

References

Aouay, M., Magnin, A., Putaux, J.L., Boufi, S., 2022. Biobased nucleation agents for poly-L-(lactic acid) — Effect on crystallization, rheological and mechanical properties. Int. J. Biol. Macromol. 218, 588–600. https://doi.org/10.1016/J.IJBIOMAC.2022.07.069

Arao, Y., Fujiura, T., Itani, S., Tanaka, T., 2015. Strength improvement in injection-molded jute-fiber-reinforced polylactide green-composites. Compos. Part B Eng. 68, 200–206. https://doi.org/10.1016/J.COMPOSITESB.2014.08.032

Cao, X., Wang, Y., Chen, H., Hu, J., Cui, L., 2021. Preparation of different morphologies cellulose nanocrystals from waste cotton fibers and its effect on PLLA/PDLA composites films. Compos. Part B Eng. 217, 108934. https://doi.org/10.1016/J.COMPOSITESB.2021.108934

Clarkson, C.M., El Awad Azrak, S.M., Schueneman, G.T., Snyder, J.F., Youngblood, J.P., 2020. Crystallization kinetics and morphology of small concentrations of cellulose nanofibrils (CNFs) and cellulose nanocrystals (CNCs) melt-compounded into poly(lactic acid) (PLA) with plasticizer. Polymer 187, 122101. https://doi.org/10.1016/J.POLYMER.2019.122101

Espino-Pérez, E., Bras, J., Ducruet, V., Guinault, A., Dufresne, A., Domenek, S., 2013. Influence of chemical surface modification of cellulose nanowhiskers on thermal, mechanical, and barrier properties of poly(lactide) based bionanocomposites. Eur. Polym. J. 49, 3144–3154. https://doi.org/10.1016/J.EURPOLYMJ.2013.07.017

Fortunati, E., Peltzer, M., Armentano, I., Torre, L., Jiménez, A., Kenny, J.M., 2012. Effects of modified cellulose nanocrystals on the barrier and migration properties of PLA nano-biocomposites. Carbohydr. Polym. 90, 948–956. https://doi.org/10.1016/J.CARBPOL.2012.06.025

Kulinski, Z., Piorkowska, E., 2005. Crystallization, structure and properties of plasticized poly(l-lactide). Polymer 46, 10290–10300. https://doi.org/10.1016/J.POLYMER.2005.07.101

Lim, L.T., Auras, R., Rubino, M., 2008. Processing technologies for poly(lactic acid). Prog. Polym. Sci. 33, 820–852. https://doi.org/10.1016/J.PROGPOLYMSCI.2008.05.004

Lorenzo, A.T., Arnal, M.L., Albuerne, J., Müller, A.J., 2007. DSC isothermal polymer crystallization kinetics measurements and the use of the Avrami equation to fit the data: Guidelines to avoid common problems. Polym. Test. 26, 222–231. https://doi.org/10.1016/J.POLYMERTESTING.2006.10.005

Lunt, J., 1998. Large-scale production, properties and commercial applications of polylactic acid polymers. Polym. Degrad. Stab. 59, 145–152. https://doi.org/10.1016/S0141-3910(97)00148-1

Niu, W., Guo, Y., Huang, W., Song, L., Xiao, Z., Xie, Y., Wang, Y., 2022. Aliphatic chains grafted cellulose nanocrystals with core-corona structures for efficient toughening of PLA composites. Carbohydr. Polym. 285, 119200. https://doi.org/10.1016/J.CARBPOL.2022.119200

Reid, M.S., Villalobos, M., Cranston, E.D., 2017. Benchmarking Cellulose Nanocrystals: From the Laboratory to Industrial Production. Langmuir 33, 1583–1598. https://doi.org/10.1021/ACS.LANGMUIR.6B03765

Samir, M.A.S.A., Alloin, F., Sanchez, J.Y., Dufresne, A., 2004. Cross-linked nanocomposite polymer electrolytes reinforced with cellulose whiskers. Macromolecules 37, 4839–4844. https://doi.org/10.1021/MA049504Y

Seraji, A.A., Goharpey, F., Khademzadeh Yeganeh, J., 2022. Highly crystallized and tough polylactic acid through addition of surface modified cellulose nanocrystals. J. Appl. Polym. Sci. 139, e52871. https://doi.org/10.1002/APP.52871

Shuai, C., Yuan, X., Yang, W., Peng, S., He, C., Feng, P., Qi, F., Wang, G., 2020. Cellulose nanocrystals as biobased nucleation agents in poly-l-lactide scaffold: Crystallization behavior and mechanical properties. Polym. Test. 85, 106458. https://doi.org/10.1016/J.POLYMERTESTING.2020.106458

Singh, S., Patel, M., Schwendemann, D., Zaccone, M., Geng, S., Maspoch, M.L., Oksman, K., 2020. Effect of Chitin Nanocrystals on Crystallization and Properties of Poly(lactic acid)-Based Nanocomposites. Polym. 2020, Vol. 12, Page 726 12, 726. https://doi.org/10.3390/POLYM12030726

Soulestin, J., Prashantha, K., Lacrampe, M.F., Krawczak, P., 2011. Bioplastics Based Nanocomposites for Packaging Applications. Handb. Bioplastics Biocomposites Eng. Appl. 76–119. https://doi.org/10.1002/9781118203699.CH4

Wu, J. jun, Gao, N., Jiang, L., Zhong, G. ji, Deng, C., Gao, X., 2022. The coupling effect of cellulose nanocrystal and strong shear field achieved the strength and toughness balance of Polylactide. Int. J. Biol. Macromol. 207, 927–940. https://doi.org/10.1016/J.IJBIOMAC.2022.03.172

Yin, Y., Tian, X., Jiang, X., Zhu, P., 2022. Modification of cellulose nanocrystals via surface-initiated ARGET ATRP and their reinforcement of poly(lactic acid)-based biocomposites. Ind. Crops Prod. 188, 115575. https://doi.org/10.1016/J.INDCROP.2022.115575

Yu, H.Y., Zhang, H., Song, M.L., Zhou, Y., Yao, J., Ni, Q.Q., 2017. From Cellulose Nanospheres, Nanorods to Nanofibers: Various Aspect Ratio Induced Nucleation/Reinforcing Effects on Polylactic Acid for Robust-Barrier Food Packaging. ACS Appl. Mater. Interfaces 9, 43920–43938. https://doi.org/10.1021/ACSAMI.7B09102

Supplementary material

Isothermal crystallization analysis

The process of isothermal crystallization was carried out in the following manner: (i) the samples were heated to 200 °C for 5 min to erase the thermal history, (ii) quenched at a rate of 50 °C min^{-1}, (iii) reheated to the desired isothermal temperature (T_c = 115, 120 and 125 °C) at a rate of 10 °C min^{-1}, and (iv) kept at this temperature for 30 min to guarantee the full crystallization from the latent melt.

To conduct the Avrami analysis, **Eq. S1** was employed to determine the relative crystallinity conversion (χ_c).

$$\chi_c = \frac{\Delta H(t)}{\Delta H_{total}} \quad \textbf{(S1)}$$

In order to analyze the isotherms, a plugin developed by Lorenzo et al. (Lorenzo et al., 2007) for Avrami study was used in the Origin software. The proportion of crystalline material (w_c) is directly proportional to χ_c, while the volume fraction of transformed material (V_c) can be determined using **Eq. S2**. The amorphous and crystalline PLLA densities were presumed to be ρ_a = 1.25 g cm^{-3} and ρ_c =1.359 g cm^{-3}, respectively. Finally, Avrami plots were generated by applying **Eq. S4**.

$$V_c = \frac{W_c}{Wc+\left(\frac{\rho_c}{\rho_a}\right).(1-W_c)} \quad \textbf{(S2)}$$

$$1 - V_c(t) = e^{(-kt^n)} \quad \textbf{(S3)}$$

$$Log\left(-Ln\left(1 - V_c(t)\right)\right) = Log(k) + nLog(t) \quad \textbf{(S4)}$$

The crystallization half-time ($t_{1/2}$) was calculated using **Eq. S5**:

$$t_{1/2} = \left(\frac{ln2}{k}\right)^{1/n} \quad \textbf{(S5)}$$

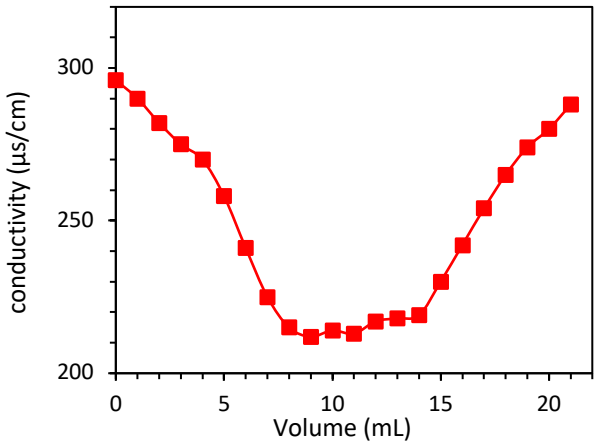

Figure S1: Representative example of conductometric titration of Am-CNCs with 5.10^{-3} M NaOH.

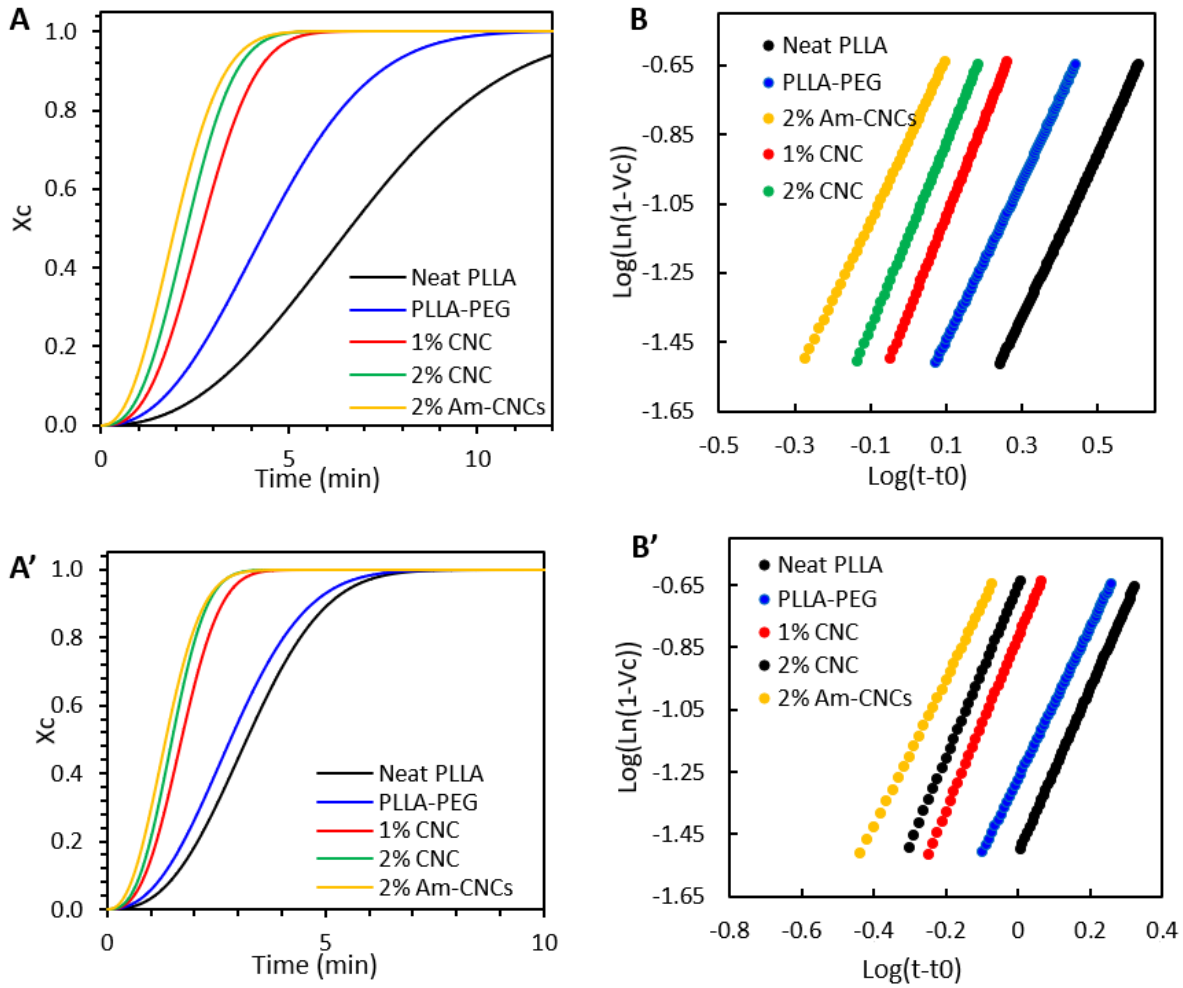

Figure S2: Evolution of Avrami analysis using isothermal data: (A,A') Plot of the extent of crystallization conversion against experimental time and (B,B') Avrami-type graph of Log(Ln(1-V_c)) versus Log(t-t_0) at temperatures of 120 and 115°C, respectively.

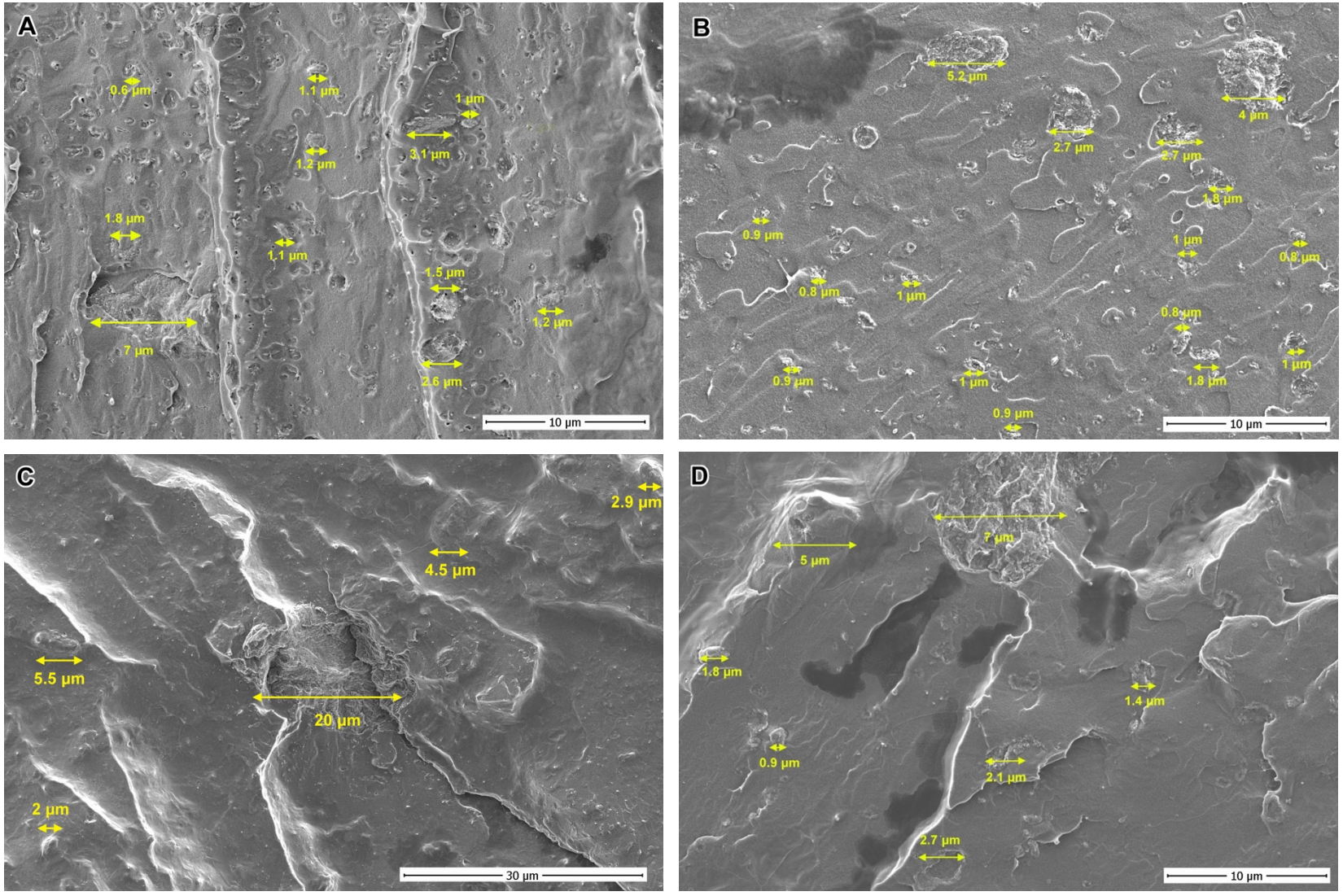

Figure S3: SEM images of the cross-sections of cryofractured PLLA/PEG composite films with indication on the size of some particle aggregates: (A) 2 wt% CNCs, (B) 2 wt% Am-CNCs, (C) 4 wt% CNCs, and (D) 4 wt% Am-CNCs. Aggregates smaller than 0.5 µm are not indicated.